



HAL
open science

Effect of kappa carrageenan on acid-induced gelation of whey protein aggregates. Part II: Microstructure

Dasong Liu, Peng Zhou, Taco Nicolai

► **To cite this version:**

Dasong Liu, Peng Zhou, Taco Nicolai. Effect of kappa carrageenan on acid-induced gelation of whey protein aggregates. Part II: Microstructure. Food Hydrocolloids, 2020, 102, pp.105590. 10.1016/j.foodhyd.2019.105590 . hal-03026673

HAL Id: hal-03026673

<https://hal.science/hal-03026673>

Submitted on 3 Dec 2020

HAL is a multi-disciplinary open access archive for the deposit and dissemination of scientific research documents, whether they are published or not. The documents may come from teaching and research institutions in France or abroad, or from public or private research centers.

L'archive ouverte pluridisciplinaire **HAL**, est destinée au dépôt et à la diffusion de documents scientifiques de niveau recherche, publiés ou non, émanant des établissements d'enseignement et de recherche français ou étrangers, des laboratoires publics ou privés.

1 **Effect of Kappa Carrageenan on Acid-induced Gelation of Whey Protein**
2 **Aggregates. Part II: Microstructure**

3

4 Dasong Liu^{a,b}, Peng Zhou^a, Taco Nicolai^{b,*}

5 ^a*State Key Laboratory of Food Science and Technology, Jiangnan University, Wuxi, Jiangsu Province*
6 *214122, China*

7 ^b*Le Mans Université, IMMM UMR-CNRS 6283, Polymères, Colloïdes et Interfaces, 72085 Le Mans*
8 *cedex 9, France*

9 *Email: Taco.nicolai@univ-lemans.fr*

10

11 **Abstract**

12 The influence of κ -carrageenan (KC) was investigated on the microstructure of gels formed
13 by acid-induced gelation of whey protein aggregates (WPA). In part I of this two-part series
14 we discussed results obtained by potentiometric titration, rheology and turbidimetry. Here we
15 report on the microstructure of both the proteins and the polysaccharides using confocal laser
16 scanning microscopy with different fluorescent labels for each type of biopolymer. The effect
17 of KC concentration at fixed net protein charge densities (α) and the effect of α at fixed KC
18 concentrations were studied. It is shown that WPA starts to form microdomains and associates
19 with KC at approximately the same α . Microstructures at steady state at different α were
20 compared with those obtained at different times during in-situ acidification after addition of
21 GDL. Significantly different microstructures were observed at elevated gelation temperatures.
22 Fluorescence recovery after photobleaching measurements showed that a significant fraction
23 of the KC chains associated with the proteins could still freely exchange even when the
24 proteins were strongly positively charged. The observations of the microstructure are
25 compared with those obtained with other experimental techniques that were reported in part I.

26 **Keywords** κ -carrageenan; whey protein; complex; gel; microstructure

27

28 **1. Introduction**

29 Gelation of proteins is an important method to texture food products. Often
30 polysaccharides are present as well as proteins. Polysaccharides can form gels by themselves,
31 but even if they don't gel themselves they may still influence the gelation process of the
32 proteins and thereby influence the texture of the food products. Polysaccharides can also be
33 added on purpose in order to obtain a more desirable texture. It is therefore of importance to
34 investigate the interaction between proteins and polysaccharides during gelation of the
35 former. Native globular proteins in aqueous solution can form a gel when they are denatured,
36 which is usually done by heating (Brodkorb, Croguennec, Bouhallab and Kehoe, 2016;
37 Nicolai, 2019) . However, suspensions of globular proteins aggregates formed by preheating
38 can be induced to form a gel by reducing the electrostatic interactions even at low
39 temperatures (Bryant and McClements, 1998; Kharlamova, Chassenieux and Nicolai, 2018;
40 Kharlamova, Nicolai and Chassenieux, 2018) , which is useful for certain applications.

41 We have conducted an extensive investigation of the influence of adding the anionic
42 polysaccharide κ -carrageenan (KC) on the acid-induced gelation of whey protein aggregates
43 (WPA). By decreasing the pH the strongly net negative charge density of the proteins is
44 reduced, which drives association of the WPA, and if the protein concentration is sufficiently
45 high, a self supporting gel is formed. Elsewhere, we reported on potentiometric titration,
46 rheology and turbidimetry measurements, which we refer to as part I (Liu, Zhou, Nicolai,
47 2020). We showed with potentiometric titration that addition of KC strongly influences the
48 relationship between the pH and the net charge of the proteins (α) for $\alpha > -2$, due to the
49 formation of complexes between the proteins and KC. We note that complexation occurred
50 even if WPA and KC have both a net negative charge. It is important to realize that the
51 parameter that controls the interaction between the biopolymers is α and not the pH. The
52 value of α was varied in-situ by adding glucono- δ -lactone (GDL) and can be deduced from
53 the amount of added GDL and measurements of the pH as was described in detail in part I.

54 Oscillatory shear measurements showed that gels were formed starting at a critical
55 charge density and that gelation was accompanied by increase of the turbidity. Adding more
56 than 1 g/L KC to 20 g/L WPA led to a strong decrease of the gel stiffness and a strong
57 increase of the turbidity. The effect of the temperature was also investigated and showed that
58 stiffer and more turbid gels were formed at higher temperatures. The gelation rate increased
59 strongly with increasing temperature and was controlled by the degradation rate of GDL, i.e.
60 the rate at which α changed. Confocal scanning microscopy (CLSM) images of acid-induced

61 WPA gels in the presence of KC reported in the literature (de Jong and van de Velde, 2007)
62 showed that the presence of KC induced formation of gels with a coarser microstructure. This
63 can explain the increase of the turbidity in the presence of KC. It was speculated that the
64 effect of KC on WPA gelation was caused by segregative microphase separation between KC
65 chains and the associating WPA followed by binding of KC to the WPA network.

66 However, in earlier studies of the microstructure of the mixed gels only the proteins
67 were visualized. Here we report on the microstructure of the gels using CLSM with different
68 fluorescent labels for the proteins and the polysaccharides, which allowed us to localize each
69 biopolymer in the mixtures. In this manner we were able to assess if and to what extent
70 microphase separation has occurred and importantly how much KC is co-localized with the
71 proteins as a function of α and time. Co-localization doesn't imply that the polysaccharides
72 are actually strongly bound. Therefore, fluorescence recovery after photobleaching (FRAP)
73 measurements were done, which allowed us to determine the fraction of strongly bound
74 immobile KC.

75 **2. Materials and Methods**

76 For the preparation and characterization of the WPA and the KC samples we refer to
77 part I. Briefly, mixtures of WPA and KC were prepared from stock solutions at the desired
78 concentration. A GDL solution at 1 M was prepared by adding water to the GDL powder.
79 After stirring for 1 min to dissolve all the GDL powder, aliquots of the GDL solution were
80 added to the biopolymer solutions while stirring. The values of α at steady state were
81 calculated using the relationship between the pH and α established by potentiometric titration
82 measurements that were reported in part I. The proteins were physically labelled by adding a
83 small amount of Rhodamin B. The polysaccharides were covalently labelled with FITC
84 following the method described by Heilig et al. (Heilig, Göggerle and Hinrichs, 2009) with
85 minor modifications as described by Bui et al. (Bui, Nguyen, Nicolai and Renou, 2019) . The
86 molar mass of the KC was not significantly modified by the labelling.

87

88 **2.1. CLSM and FRAP**

89

90 Mixtures of WPA and KC with a small fraction of labelled KC were prepared from
91 stock solutions and subsequently the required amount of GDL was added as described in part
92 I. The solutions were inserted between a concave slide and a cover slip that were hermetically

93 sealed with an adhesive Gene Frame[®] (ABgene[®], Epsom, UK). CLSM observations were
94 made at 20°C with a Zeiss LSM800 (Jena, Germany). The images with a pixel size of 70 nm
95 were obtained with a 63x water immersion objective with a numerical aperture of 1.3. It took
96 0.3 s to obtain one image. An excitation wavelength of 561 nm and detection wavelengths
97 above 550 nm were used for the Rhodamine B channel, whereas an excitation wavelength of
98 488 nm and detection wavelengths below 520 nm were used for the FITC channel. The
99 concentration of labelled KC added in all cases was 0.25 g/L. At this small concentration of
100 labelled KC the microstructure observed with the protein signal was the same as without
101 labelled KC at the same total KC concentration. Care was taken not to saturate the detection
102 so that the measured intensity was proportional to the biopolymer concentration.

103 Histograms of the fluorescence intensity distribution were obtained using the Image-J
104 programme and the relative standard deviation was calculated as the standard deviation
105 divided by the average intensity. The standard deviation of the histograms depends on the
106 overall intensity of the images, which in terms depends on the gain, laser intensity and
107 fluorescent probe concentration. However, normalizing the standard deviation by the average
108 intensity of the images renders it independent of these parameters and only a function of the
109 microstructure. The ratio of the intensities of the pores and the network was obtained by
110 measuring the intensity of many small circular areas with a diameter of 5 µm in different parts
111 of the pores and the protein network. Care was taken to sample only within the protein
112 network sections that were in focus and to minimize the inclusion of edges.

113 FRAP measurements were done following the method of Bui et al. (2019) with minor
114 modifications. Circular areas with diameter $w = 10 \mu\text{m}$ were bleached and the recovery of the
115 fluorescence intensity with time of the area was measured. One pre-bleach image and one
116 bleach image were taken followed by 6 post-bleach images at time intervals of 5 s, 6 images
117 at time intervals of 50 s and 11 images at time intervals of 500 s. In this manner the recovery
118 was probed on a logarithmic time scale. Consecutive imaging with very short time intervals
119 (0.3 s) of non-bleached images showed that no significant bleaching occurred during detection
120 of the recovery.

121

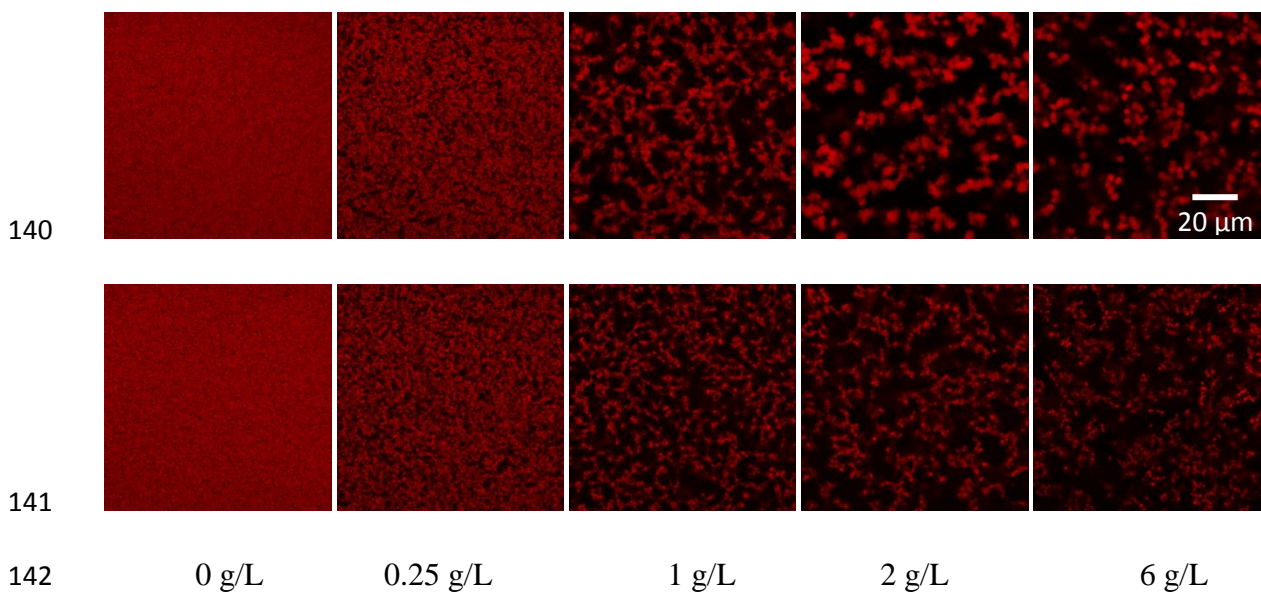
122 **3. Results and Discussion**

123 **3.1 Effect of the KC concentration**

124 The effect of the KC concentration up to 6 g/L on the microstructure of the protein
125 gels at steady state was studied for gels formed in the presence of 9 mM GDL at $C_{WP}=20 \text{ g/L}$.

126 At this concentration of GDL the steady state value of α was close to zero and very little
 127 dependent on the KC concentration, whereas the pH varied between 4.9 and 5.1. Fig. 1
 128 compares CLSM images formed at 20°C or 80°C, but visualized at 20°C. The turbidity of gels
 129 formed at 80°C did not change during cooling to 20°C and it is therefore reasonable to assume
 130 that the structure observed at 20°C is the same as at 80°C where it was formed. At both
 131 temperatures the heterogeneity of the gels increased with increasing KC concentration until
 132 about 1 g/L, but adding more KC did not appear to have a significant influence on the
 133 microstructure. For $C_{KC} \geq 1$ g/L the gels appear to consist of approximately spherical domains
 134 that are crosslinked into a network. The effect of KC on the microstructure shown in figure 1
 135 is similar to that shown by (de Jong and van de Velde, 2007) for gels formed at 20°C, at C_{WP}
 136 = 30 g/L and at a fixed pH 4.8. Interestingly, the transition to the formation of microdomains
 137 corresponds approximately to the transition between dilute and semi-dilute KC solutions
 138 (Croguennoc, Meunier, Durand and Nicolai, 2000) .

139

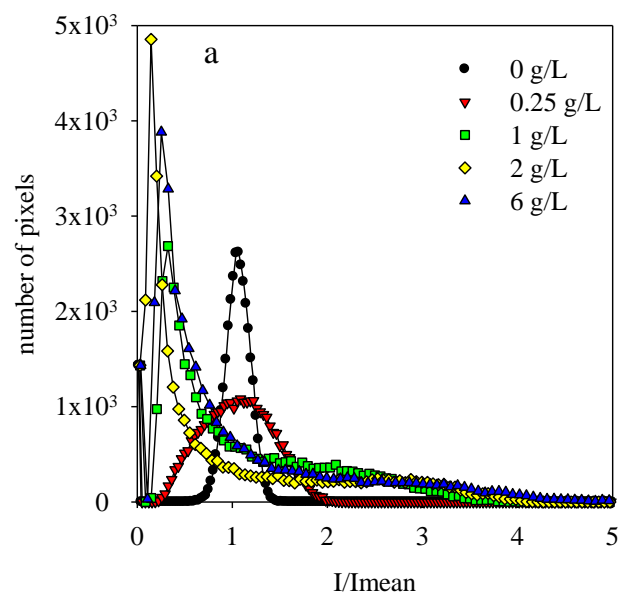


143 Fig. 1 CLSM images of gels formed after heating at 20°C (top) and 80°C (bottom) by
 144 mixtures of 20 g/L WPA and different KC concentrations. The steady state value of α was
 145 close to zero. The fluorescence of the proteins is indicated by the bright (red) colouring.

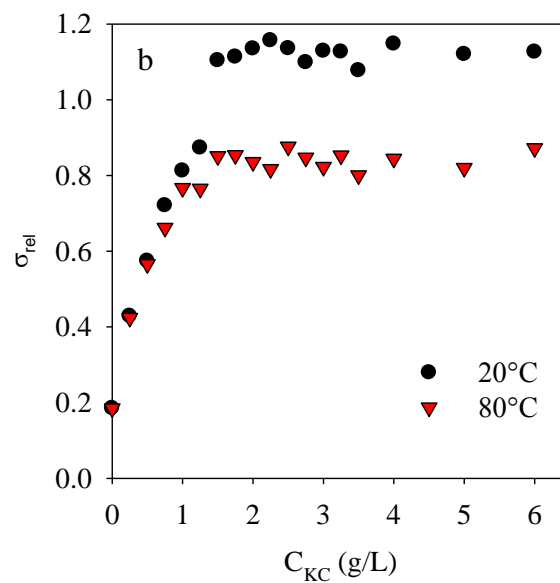
146

147 One method to quantify the heterogeneity of the microstructure is to calculate the
 148 histogram of the fluorescence intensities. They show a broadening with increasing KC

149 concentration and for $C_{KC} \geq 1$ g/L the histogram splits between a narrow high amplitude
 150 distribution at $I/I_{\text{mean}} < 1$ and a broad low amplitude distribution in the range $I/I_{\text{mean}} = 1 - 5$,
 151 see Figure 2a. This implies that for $C_{KC} \geq 1$ g/L phase separation has occurred on length
 152 scales accessible to CLSM In Figure 2b we compare the dependence of the standard deviation
 153 of the histograms normalized by the mean intensity (σ_{rel}) as a function of C_{KC} for gels formed
 154 at 20°C and at 80°C. σ_{rel} increased steeply with increasing KC concentration up to 1.5 g/L and
 155 then remained constant. Up to $C_{KC} = 1$ g/L the effect of temperature was weak, but at higher
 156 KC concentrations, σ_{rel} was larger for gels formed at 20°C.



157



158

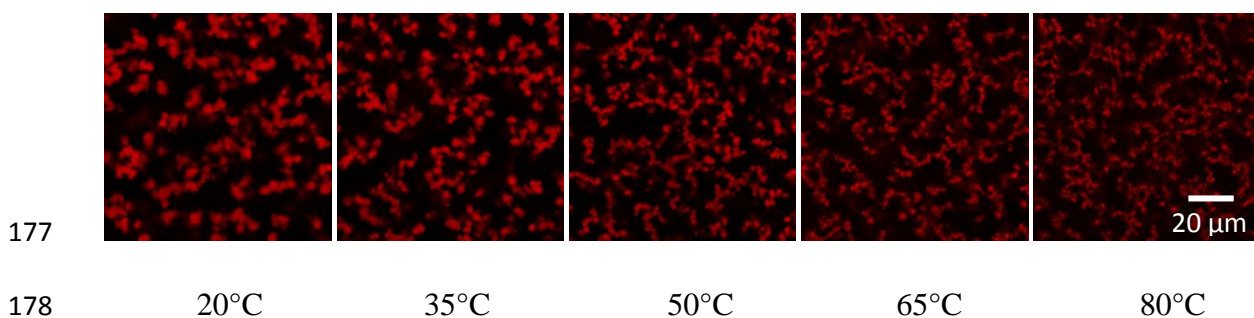
159 Fig. 2a Histograms of the fluorescence intensity relative to the average intensity for gels of
160 the images shown in fig. 1.

161 Fig. 2b Comparison of the dependence of the relative standard deviation, i.e. the standard
162 deviation of the intensity histogram normalized by the mean intensity, on the KC
163 concentration for gels formed at 20°C and 80°C.

164

165 3.2 Effect of the temperature

166 The effect of the temperature on the microstructure of the gels was explored in more
167 detail for mixtures containing 1, 2 and 4 g/L KC. Figure 3 shows CLSM images for mixtures
168 at $C_{KC} = 2$ g/L formed at different temperatures. They confirm the impression that the gel
169 structure becomes less heterogeneous when formed at higher temperatures. Figure 4 shows
170 that σ_{rel} dropped sharply above 50 °C both at $C_{KC} = 2$ g/L and 4 g/L, but was almost
171 independent of the temperature at $C_{KC} = 1$ g/L. The results also show that the structure
172 becomes independent of the KC concentration for $C_{KC} \geq 1.5$ g/L at all temperatures. De Jong et
173 al. (2009) compared the microstructure of gels at $C_{WP} = 30$ g/L formed at 25°C and 37°C in
174 the presence of 5 g/L KC and found very little difference in agreement with the present
175 results. However, here we find that for $C_{KC} > 1$ g/L there is a significant effect of the
176 temperature above 50°C leading to formation of smaller protein domains.



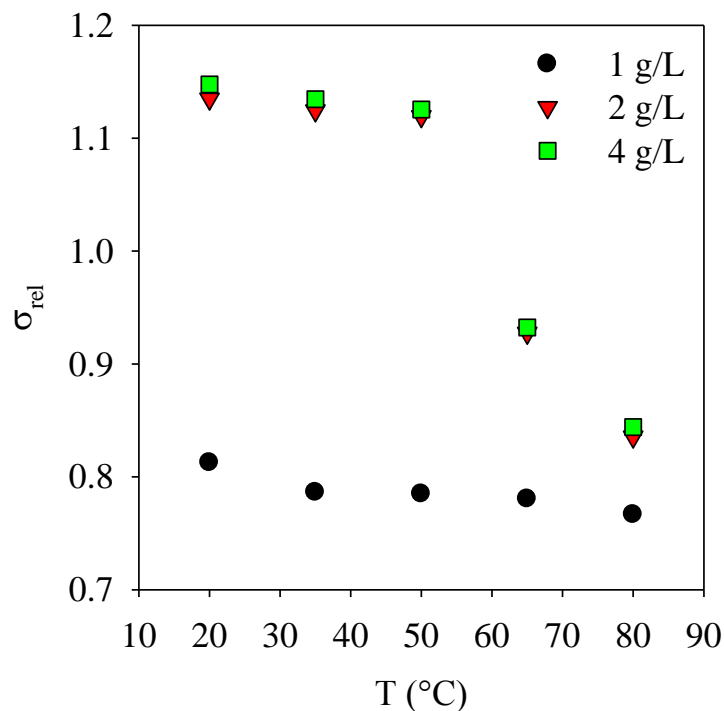
179 Fig. 3 CLSM images of gels formed after heating at different temperatures by mixtures of 20
180 g/L WPA and 2 g/L KC. The steady state value of α was close to zero.

181

182 In part I we showed that the gel stiffness increased significantly with increasing
183 gelation temperature for $C_k \geq 2$ g/L. Here we find that smaller microdomains were formed at
184 higher temperatures suggesting that the two phenomena are related. However, whereas the gel

185 stiffness increased progressively with increasing gelation temperature, the microstructure
186 changed only significantly above 50 °C. It is therefore not straightforward to relate the gel
187 stiffness to the microstructure. We note that the turbidity at $C_{KC} = 2$ g/L actually increased
188 with increasing temperature, see figure 12a of part I, whereas the size of the microdomains
189 decreased. This illustrates that the relationship between the turbidity and the microstructure as
190 probed by CLSM is not straightforward.

191



192

193 Fig.4 Dependence of the relative standard deviation, i.e. the standard deviation of the intensity
194 histogram normalized by the mean intensity, on the temperature of gelation for gels formed by
195 mixtures of 20 g/L WPA and different KC concentrations. The steady state value of α was
196 close to zero.

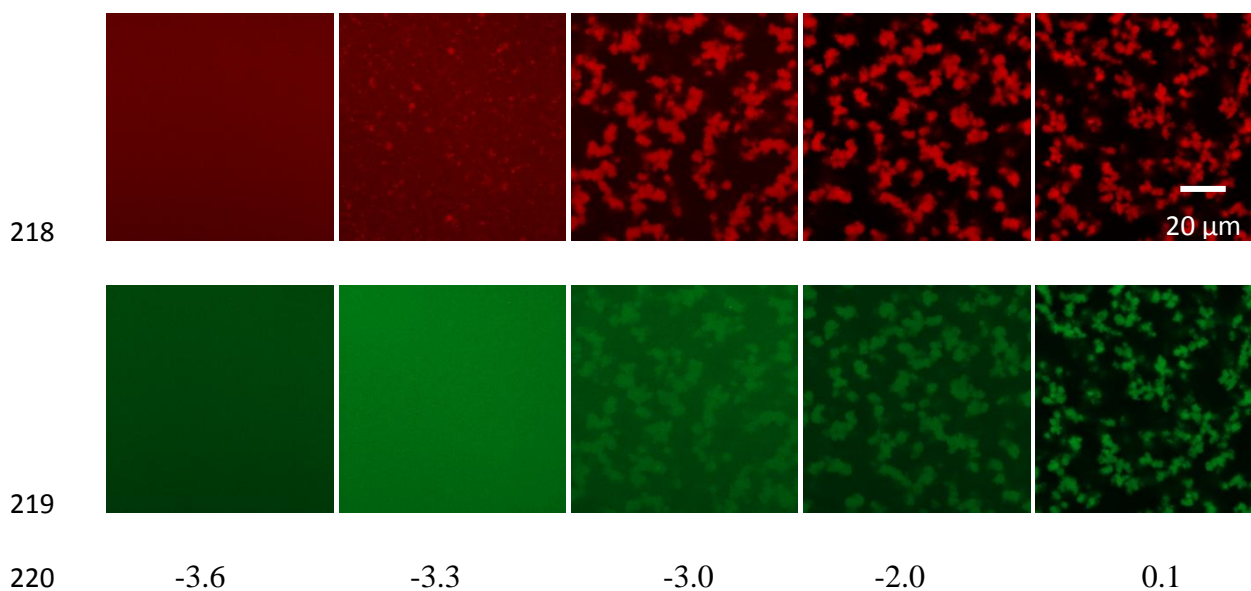
197

198 3.3 Complexation between KC and WPA

199 A crucial issue is whether and to what extent KC binds to the protein gel. As was
200 mentioned in the introduction, titration measurements show a clear influence of the presence
201 of KC for $\alpha > -2.0$, which indicates that complexes are formed between the two types of

202 biopolymers. However, this measurement cannot show the extent to which KC is bound to the
203 protein gels at different α . KC can be localized within the gels using CLSM by covalently
204 labelling KC with a fluorescent probe different from the one used to label the protein and its
205 fluorescence was detected at different wavelengths.

206 Figure 5 shows CLSM images of mixtures of 20 g/L WPA and 2 g/L KC that have
207 reached steady state at 20°C after addition of different amounts of GDL corresponding to
208 different steady state values of α . The correspondence between α and the pH was shown in
209 part I. The microstructures of the proteins and KC was visualized separately and compared.
210 At $\alpha = -3.6$ the microstructure of both biopolymers was homogeneous on length scales
211 accessible to CLSM. At $\alpha = -3.3$, protein rich domains could be observed, but KC still
212 appeared homogeneously distributed. At $\alpha = -3.0$ the protein network structure was distinctly
213 visible and the same network structure could also be seen with the signal corresponding to KC
214 implying that KC was bound to the proteins. However, still much of the KC was
215 homogeneously distributed. As α was further increased a larger fraction of KC became bound
216 to the protein network. This visual impression is confirmed by co-localisation plots of the KC
217 signal vs the protein signal, see Figure S1 of the supplementary information.

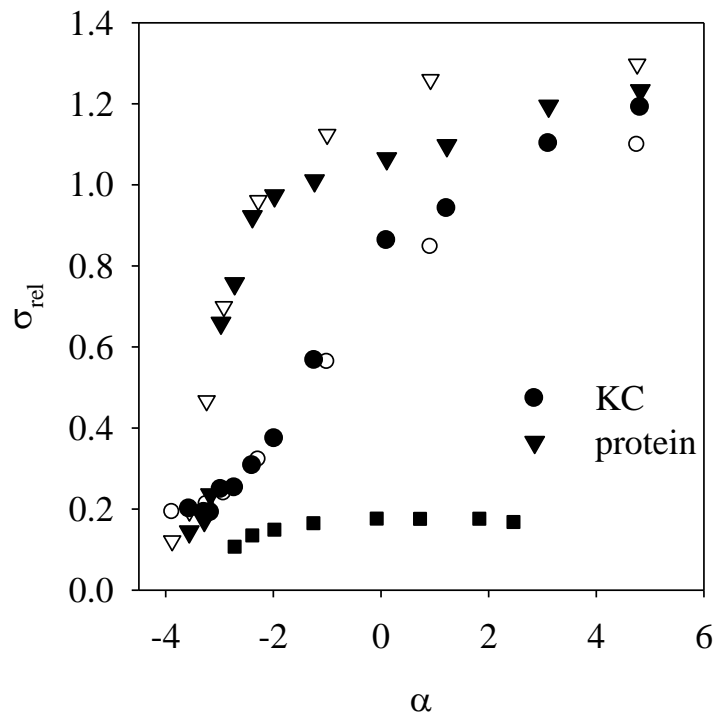


221 Fig. 5 CLSM images of gels formed at 20°C after adding different amounts of GDL resulting
222 in different steady state values of α indicated in the figure. The distribution of proteins
223 indicated in red is shown in the top row and that of KC indicated in green is shown in the
224 bottom row.

225

226 The fact that the KC is co-localized with the protein domains implies attractive
227 interaction between the two biopolymers that is strong enough to overcome the mixing
228 entropy that drives KC to be homogeneously distributed. We do not believe that the attractive
229 interaction is caused by the labeling of KC as the protein microstructure was the same as with
230 unlabelled KC. Furthermore, binding of KC was progressive with increasing α and we
231 showed elsewhere that KC with the same labelling actually segregated from the protein
232 domains at neutral pH (Nguyen, B. T., Nicolai, T., Chassenieux, C. & Benyahia, L. (2014)).

233 The dependence of σ_{rel} on α for the proteins and KC is compared in Figure 6. Below α
234 = -3.3, the CLSM images were visually homogeneous with values of σ_{rel} between 0.12 and
235 0.22. For the proteins σ_{rel} started to increase strongly with increasing α at $\alpha = -3.3$, which is
236 caused by the association of WPA and formation of a heterogeneous gel. This initial steep
237 increase was followed by a weak increase for $\alpha > -2.4$. The protein structure is strongly
238 influenced by the presence of KC at all α as σ_{rel} remains small in the absence of KC, see
239 Figure 6. If all KC is bound to the protein, σ_{rel} should be the same for both biopolymers. This
240 is clearly not the case as σ_{rel} corresponding to KC increased much more progressively with α
241 and approaches the value of the proteins only at large α .

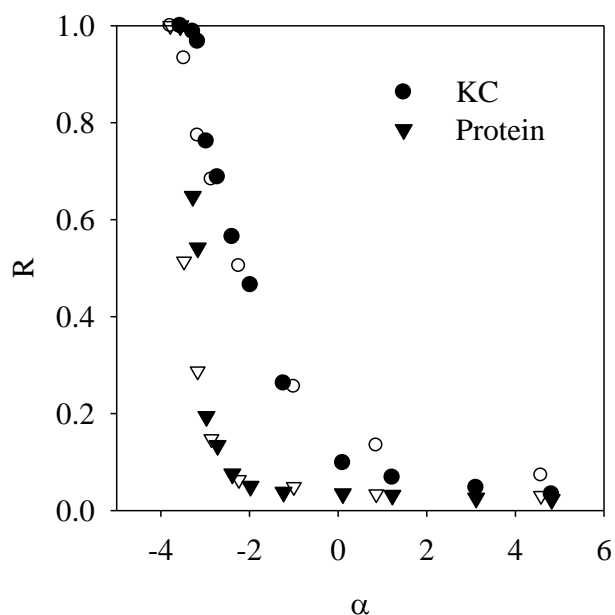


242

243 Fig.6 Dependence on the net protein charge density of the relative standard deviation of the
 244 protein (triangles) and KC (circles) intensity distributions for mixtures of 20 g/L WPA and 2
 245 g/L KC at steady state after addition of different amounts of GDL (filled symbols). Results
 246 derived from the time dependence, see text, are shown as open symbols. For comparison the
 247 relative standard deviations obtained for pure protein gels are also shown (squares).

248

249 For a more direct measure of the partition of each biopolymer between the gel and the
 250 sol fraction, we measured the ratio (R) of the intensity in the pores over that of the network.
 251 The assumption is that all fluorescent probes are bound to the biopolymers and that the sol
 252 fraction within the network structure is negligible. The dependence of R on α is shown in
 253 figure 7. R was unity for the proteins at $\alpha = -3.6$ where no dense domains could be detected,
 254 but it decreased steeply with increasing α to $R = 0.05$ at $\alpha = -2$. For KC, R started to decrease
 255 at the same value of α , but the decrease was more progressive reaching a value of 0.1 at $\alpha =$
 256 0.1. At $\alpha = -2.4$, when the protein network was already fully formed and contained almost all
 257 of proteins, R was still as high as 0.6 for KC, i.e. most of the KC was still free in solution.



258

259 Fig. 7 Dependence on α of the ratio of the protein and KC fluorescence intensities in the sol
 260 and the gel phase for mixture of 20 g/L WPA and 2 g/L KC at steady state after addition of
 261 different amounts of GDL (filled symbols). Results derived from the time dependence, see
 262 text, are shown as open symbols.

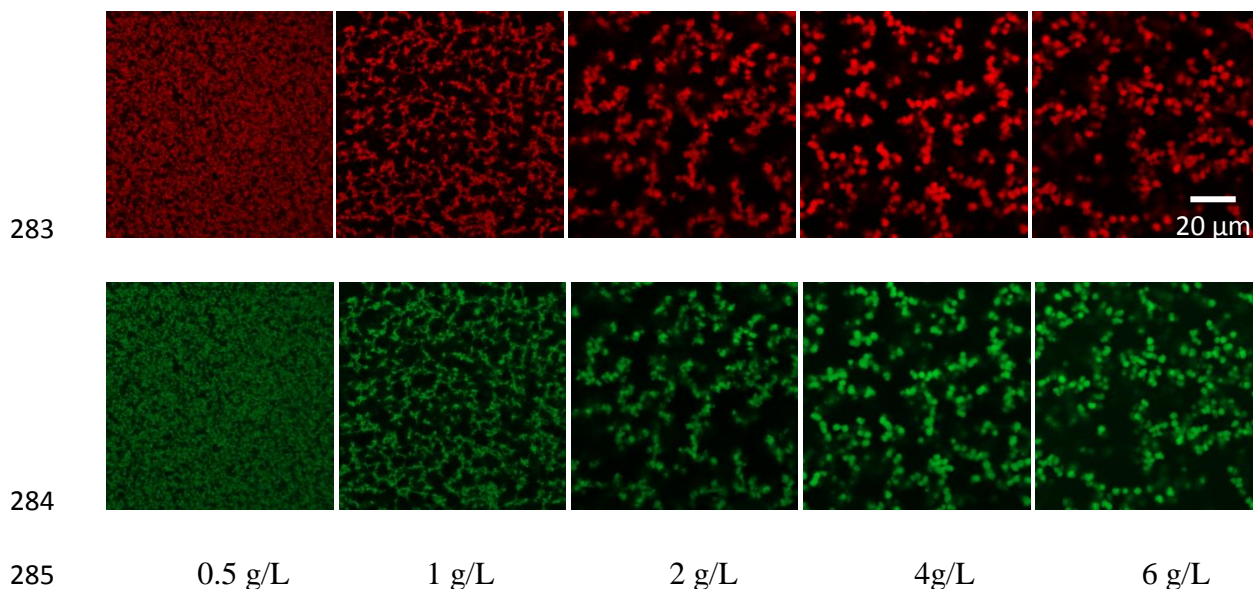
263

264 We may compare these results with rheology and turbidity results reported in part I.
 265 The rise in the turbidity started at the same value of α as where σ_{rel} increased and was caused
 266 by the formation of the microdomains. The increase of the storage shear modulus also started
 267 at approximately the same value of α , which means that the critical value of α where
 268 microdomains are formed and where these domains start to connect into a space filling
 269 network are very close.

270 The effect of the KC concentration on the partition of the biopolymers in gels formed
 271 at 20°C was investigated at $\alpha \approx 3$ where the values of σ_{rel} for the protein and polysaccharide
 272 signal were close at $C_{KC} = 2$ g/L and R was small for both biopolymers. CLSM images
 273 showed a similar dependence of the microstructure on the KC concentration at $\alpha \approx 3$ as at $\alpha =$
 274 0, see figure 8. Comparison of the protein and KC signals shows that at this charge density the
 275 KC was co-localized with the proteins at all KC concentrations. This was confirmed by the
 276 values of σ_{rel} that were close for both biopolymers and the low values of R for both
 277 biopolymers, see figure 9. However, whereas the values of σ_{rel} for the proteins remained

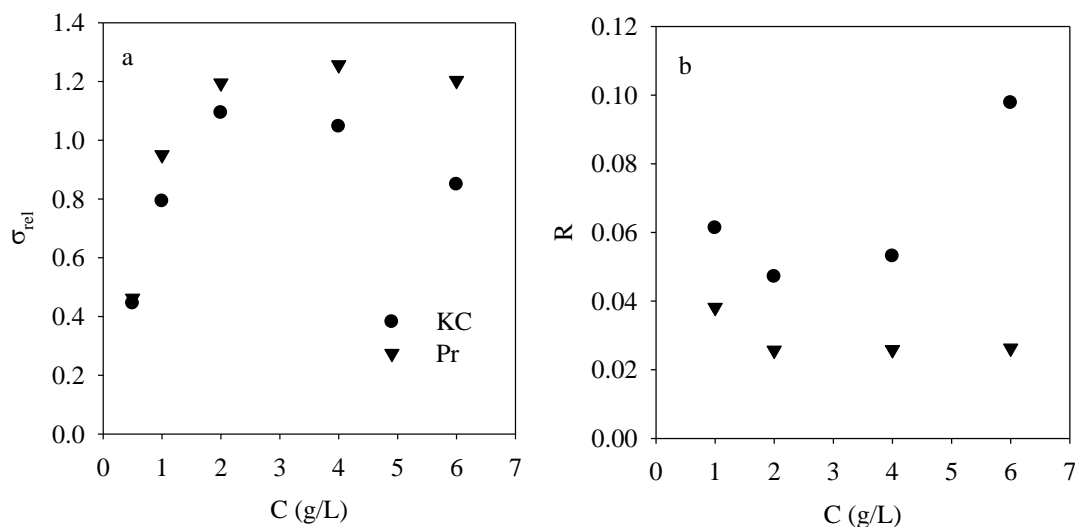
278 approximately the same, σ_{rel} of the KC signal decreased weakly between 4 and 6 g/L KC and
 279 R increased by a factor two from 0.05 to 0.1. The titration measurements discussed in part I
 280 suggest that for $C_{KC} > 4$ g/L the proteins started to become saturated with KC, which may
 281 explain why more free KC was observed within the pores.

282



286 Fig. 8 CLSM images of mixtures of 20 g/L WPA and different concentrations of KC at $\alpha \approx$
 287 3.0. The distribution of proteins indicated in red is shown in the top row and that of KC
 288 indicated in green is shown in the bottom row.

289



291 Fig.9 Dependence of the relative standard deviation of the protein and the KC intensity
292 distributions (a) and the ratio of the protein and the KC intensity in the sol and the gel phase
293 (b) on the KC concentrations at $\alpha \approx 3.0$.

294

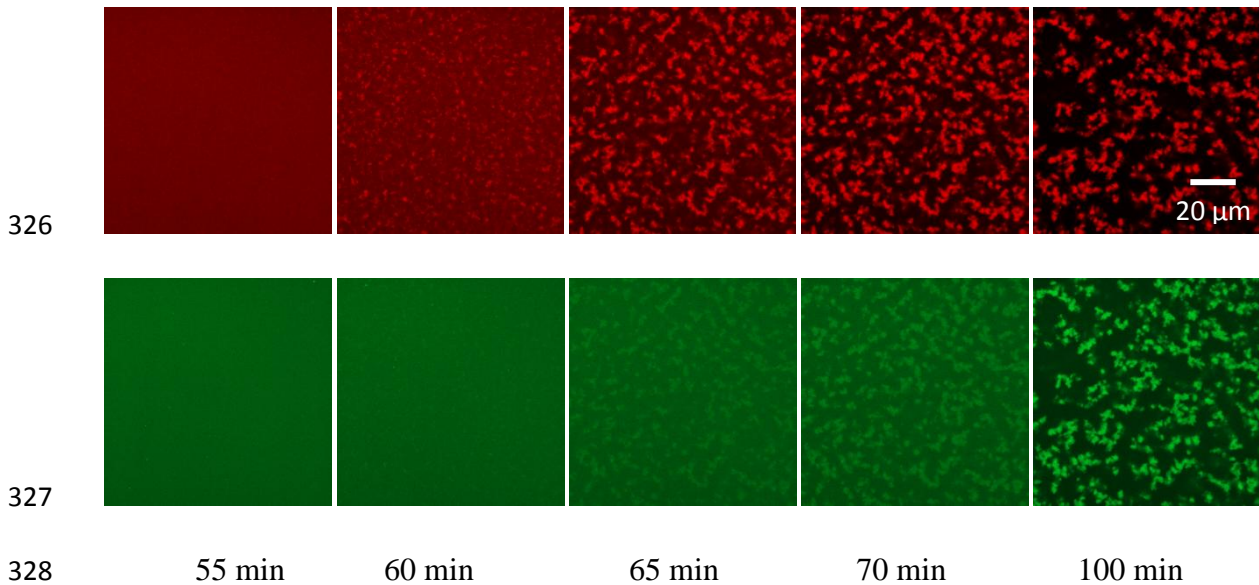
295 In part I we showed that the turbidity increased steeply up to $C_{KC} = 1$ g/L, but
296 remained approximately constant at higher concentrations. Here we find that the
297 microstructure changes strongly with increasing KC concentrations until $C_{KC} = 1$ g/L and
298 remains the same at higher concentrations, see figure 1, in agreement with the turbidity
299 measurements. However, the stiffness of the gels did not vary much with increasing KC
300 concentration until $C_{KC} = 1$ g/L and decreased steeply only at higher concentrations. It is clear
301 that the gel stiffness is not directly related to the microstructure and that one needs to consider
302 the effect on the connectivity and the bond strength as well, which is influenced by the
303 presence of KC.

304 **3.4 Evolution of the microstructure during gelation**

305 As was mentioned in the introduction, the formation of a more heterogeneous protein
306 structure in the presence of KC has been attributed to segregative phase separation between
307 the associating WPA aggregates and KC that is arrested by gelation (De Jong et al., 2009) .
308 However, it is clear from the measurements shown above that at steady state the concentration
309 of KC in the protein rich domains is not lower than that in the protein poor domains at any α ,
310 which contradicts segregative phase separation. Nevertheless, one may wonder if segregative
311 phase separation occurs during the gelation process. Therefore we studied the evolution of the
312 microstructure in-situ with CLSM during degradation of GDL. Figure 10 shows the evolution
313 of the protein and KC microstructure as a function of time at 20°C for a mixture containing 20
314 g/L WPA and 2 g/L KC. A relatively large quantity of GDL was added (22 mM) in order to
315 ensure fast gelation. Up to 55 min, the distribution of both biopolymers was homogeneous.
316 After 60 min, small dense protein domains were visible, whereas KC was still homogeneously
317 distributed. After 65 min, more protein was assembled in the form of dense domains that were
318 connected into a network. KC showed the same structure implying that KC and protein were
319 co-localized. At longer times the network structure no longer evolved much. The important
320 conclusion that can be drawn from this experiment is that at no time during the gelation
321 process does segregative phase separation occur between the protein aggregates and KC.
322 However, close to the critical value of α the WPA/KC complexes are dispersed in a semi-

323 dilute solution of free excess KC, which could drive phase separation between the complexes
324 and excess KC via depletion interaction.

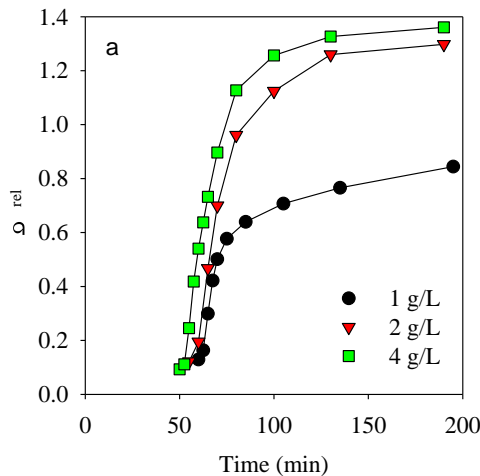
325



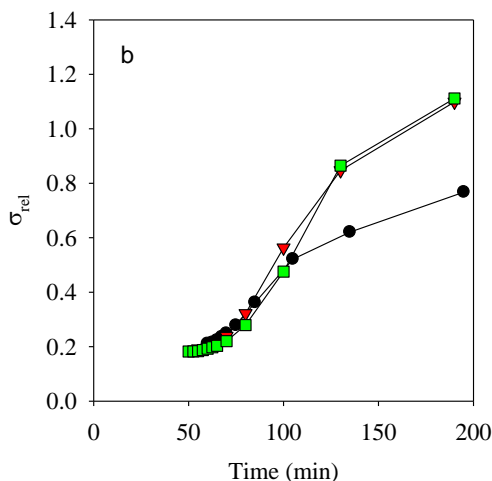
329 Fig. 10 CLSM images of mixtures of 20 g/L WPA and 2 g/L KC at different times after
330 addition of 22 mM GDL. The distribution of proteins indicated in red is shown in the top row
331 and that of KC indicated in green is shown in the bottom row.

332

333 Similar measurements were done at $C_{KC} = 1$ and 4 g/L. The evolution of σ_{rel} is shown
334 in figure 11. For the proteins, σ_{rel} increased sharply at a characteristic time (t_c) and then
335 stabilized. t_c decreased weakly with increasing KC concentration in agreement with the weak
336 decrease of the critical time where the turbidity started to increase shown in figure 11 of part
337 I. The values of σ_{rel} at long times increased with increasing KC concentration in agreement
338 with the steady state values shown in figure 2. For KC, σ_{rel} increased progressively with time
339 and approached the same values as for the proteins only at long times.



340



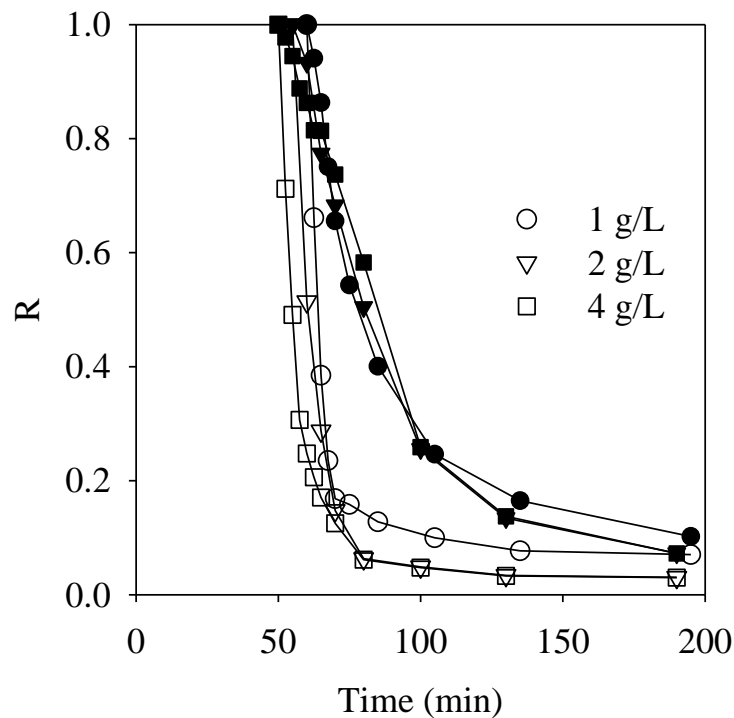
341

342 Fig. 11 Evolution of the relative standard deviation with time after addition of 22 mM GDL
 343 for the protein structure (a) and KC (b) for mixtures of 20 g/L WPA and different
 344 concentrations of KC indicated in the figure.

345

346 The evolution of the contrast in fluorescence between the pores and the network is
 347 shown in figure 12. R started to decrease at the same time for both biopolymers, but the
 348 decrease was much steeper for the proteins. It is clear that all KC is not bound immediately to
 349 the proteins, but that an increasing fraction of KC binds progressively with time to the
 350 proteins. These results as a function of time are strikingly similar to those as a function of α
 351 shown in figures 6 and 7. In part I we have shown that α is proportional to the amount of
 352 degraded GDL for $\alpha < 2$ and that the fraction of degraded GDL increases linearly with time
 353 up to a fraction of 0.5. It took 170 min to degrade half of the GDL, i.e. 11 mM in this

354 experiment. We may consider that in the relevant range of α the increase of α is proportional
 355 to the amount of degraded GDL. It follows that α increased at a rate of $0.058 \times t$, with t in
 356 minutes. Titration measurements of WPA showed that the initial value of α was -7.4 ± 0.2 , see
 357 part I. Good quantitative agreement between the dependence on time and on α at steady state
 358 was obtained if we use $\alpha(t) = -7.2 + 0.062t$, see figs 6 and 7, which is close to the calculated
 359 time dependence of α . The good superposition implies that the rate at which the
 360 microstructure evolves is limited by the evolution of α .



361
 362 Fig.12 Evolution of R with time after addition of 22 mM GDL for the proteins (open
 363 symbols) and KC (filled symbols) for mixtures of 20 g/L WPA and different concentrations of
 364 KC indicated in the figure.

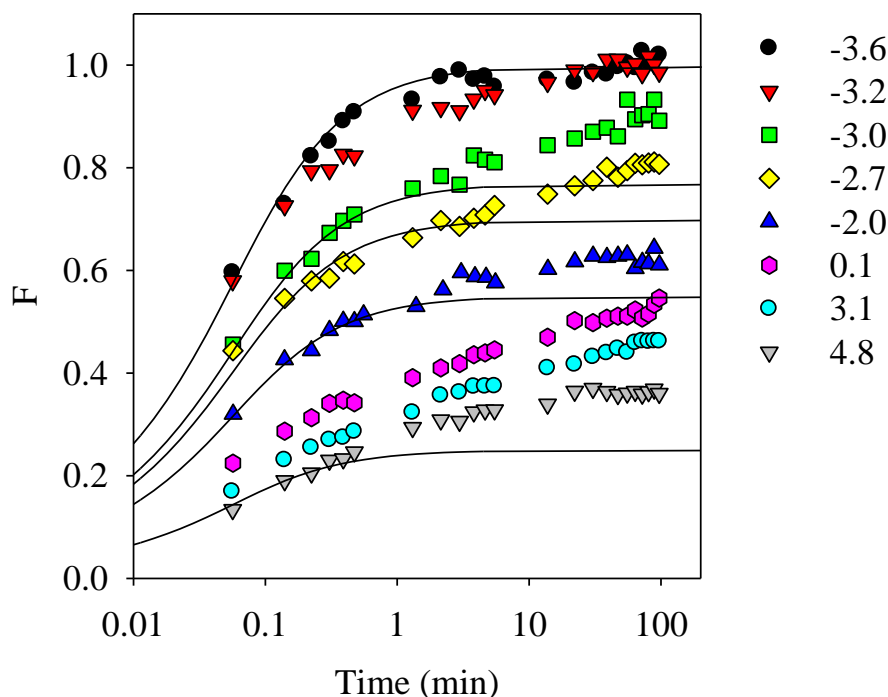
365
 366 **3.5 Mobility of KC chains**

367 We have shown above that KC becomes increasingly co-localized with the proteins
 368 with increasing α . However, CLSM images cannot show to what extent the polysaccharides
 369 are bound to the proteins or can exchange with polysaccharides elsewhere. The exchange can
 370 be probed using FRAP by bleaching small circular areas with diameter $w = 10 \mu\text{m}$ situated in

371 the network. As an example images of a gel before bleaching and at different times after
 372 bleaching is shown in Figure S2 of the supplementary information. The fluorescence recovery
 373 ($F(t)$) was calculated from the time dependent intensity ($I(t)$) as: $F(t) = (I(t)-I(0))/(I_{int}-I(0))$,
 374 where I_{int} is the intensity before bleaching and $I(0)$ is the intensity just after bleaching. Figure
 375 13 shows examples of F for gels formed by mixtures of 20 g/L WPA and 2 g/L KC at
 376 different α . The solid line in figure 13 shows the predicted recovery for the case that it is
 377 caused by diffusion motion of the labelled chains with a single diffusion coefficient (D):

$$378 \quad F(t) = \exp(-2\tau/t)[I_0(2\tau/t)+I_1(2\tau/t)] \quad 1$$

379 where $\tau = w^2/4D$ is the characteristic time needed to diffuse out of the bleached area and I_0
 380 and I_1 are Bessel functions (Soumpasis, 1983) . At $\alpha = -3.6$ the recovery was complete and
 381 could be described in terms of a single diffusion coefficient ($D = 1.9 \times 10^{-11} \text{ m}^2/\text{s}$) indicating
 382 that the KC chains were not bound to protein domains. However, this was clearly not the
 383 case at larger α . The initial increase of F can still be described by eq. 1 with the same
 384 relaxation time, if we assume that only a fraction of KC moves freely, see solid lines in figure
 385 13. However, this initial fast recovery is followed by a very slow increase of F on logarithmic
 386 time scales. A similar behaviour has recently been reported for dextran chains in heat-set
 387 whey protein gels (Inthavong, Nicolai and Chassenieux, 2018) .

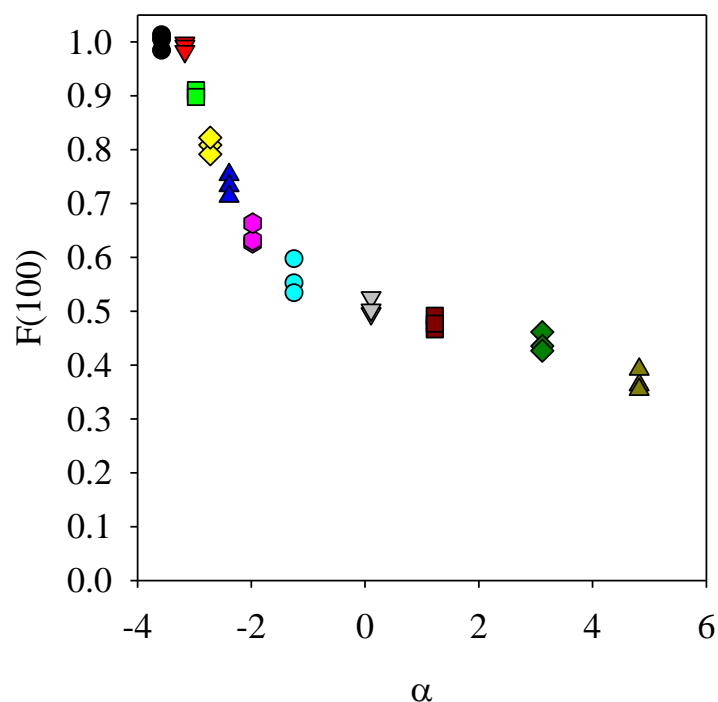


388

389 Fig. 13 Recovery of the KC fluorescence intensity for mixtures of 20 g/L WPA and 2 g/L KC
390 at different values of α indicated in the figure. Solid lines correspond to eq. 1 with $D = 1.9$
391 $\times 10^{-11}$ m²/s.

392

393 The value of F reached after 100 min ($F(100)$) decreased sharply with increasing α
394 starting at $\alpha = -3.2$ followed by a weak decrease for $\alpha > -1.5$, see figure 14. Notice that the
395 fraction of KC that diffused unhindered was less and decreased down to about 20% at $\alpha = 4.8$.
396 Figure 7 shows that at $\alpha > 0$ the KC concentration associated with the protein network was
397 more than 10 times larger than in the sol so that the contribution to F of KC in the sol can be
398 neglected. We may therefore conclude that a significant fraction of the KC that was associated
399 with the protein network remained fully mobile even at large α . Obviously, more work is
400 needed in order to elucidate the mechanism of binding and release of KC chains to the protein
401 network.



402

403 Fig. 14 Recovery of the KC fluorescence intensity after 100 min for mixtures of 20 g/L WPA
404 and 2 g/L KC as a function of α . Results are shown of measurements at three different spots
405 in the network of each gel.

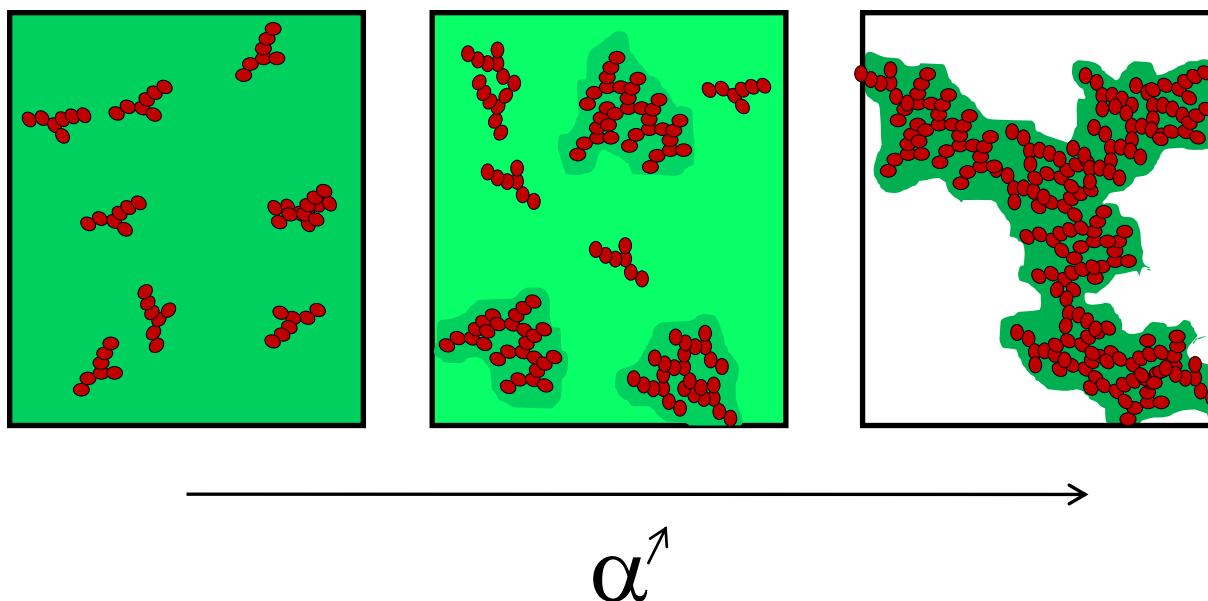
406

407 **3.6 Gelation mechanism**

408 CLSM images of the proteins and KC fluorescence show that acidification does not
409 induce segregative phase separation between KC and WPA aggregates at any value of α .
410 Instead dense protein domains are formed that contain at least as much KC as in the protein
411 poor phase. The rate at which the microstructure is formed is set by the rate at which GDL
412 degrades and therefore results as a function of α are the same whether they are obtained by
413 measuring the dependence on time or on the GDL concentration at steady state. The important
414 implication is that the microstructures observed at different α are not caused by phase
415 separation between KC and growing WPA that was arrested by gelation. The presence of KC
416 led to the formation of dense protein microdomains, but KC was not expelled from these
417 domains. In fact, binding of KC to the proteins started at the same α as where the domains
418 were formed.

419 We therefore propose the following scenario, see figure 15. Reduction of the net
420 negative charge density of the proteins below a critical value allows the WPA aggregates to
421 bind to each other and some of the KC chains become associated with the proteins. If enough
422 KC is present, free excess KC is depleted from between protein/polysaccharide complexes
423 which drives the formation of microdomains by the complexes. This process is facilitated by
424 reduction of the electrostatic repulsion between the complexes as α is increased. The
425 complexes within the microdomains crosslink so that they transform into microgels. These
426 microgels initially do not cluster together due to residual electrostatic repulsion. If α is
427 increased further more microgels are formed and a larger fraction of KC binds to the proteins.
428 In addition, the electrostatic repulsion between the microgels decreases further causing them
429 to cluster into large flocs at $C < 10$ g/L and to form a system spanning network at higher
430 protein concentrations. A significant fraction of the KC that is associated with the proteins is
431 free to exchange and another fraction can exchange very slowly, indicating that the KC chains
432 are associated with the protein network with a variety of conformations and bond strengths.

433



434 Fig. 15 Schematic representation of mixtures of WPA and KC as a function of α . The protein
 435 aggregates are indicated in red and the distribution of the KC chains is indicated in green.
 436

437

438 4. Conclusion

439 In the presence of semi-dilute solutions of KC, whey protein aggregates spontaneously
 440 assemble into microdomains when their net negative charge density is decreased below a
 441 critical value. Concomitantly, KC starts to bind to positive patches on the proteins and forms
 442 complexes. The WPA aggregates in the microdomains connect to each other and to the KC
 443 chains to form microgels. As the net negative charge decreases further the microgels crosslink
 444 and form a space filling network and progressively more KC becomes associated with the
 445 protein network. Most of the KC that is associated with the network is strongly bound when
 446 the proteins have a net positive charge density, but a significant fraction of associated KC
 447 remains mobile.

448 The changes in the gel morphology as a function of time after addition of GDL is
 449 determined by the rate at which GDL degrades. The rate of GDL degradation increases
 450 strongly with increasing temperature, which leads to the formation of gels with smaller
 451 domain sizes above 50°C presumably because microdomains have less time to develop before
 452 they crosslink.

453 Acknowledgements

454 This research was partly supported by the National Natural Science Foundation of China
455 (31901613), the China Postdoctoral Science Foundation (2018M640457) and the Jiangsu
456 Province Postdoctoral Science Foundation (2018K089C).

457

458 **References**

459 Brodkorb, A., Croguennec, T., Bouhallab, S. & Kehoe, J. J. (2016). Heat-Induced Denaturation,
460 Aggregation and Gelation of Whey Proteins, *Advanced Dairy Chemistry*(pp. 155-178), Springer

461 Bryant, C. M. & McClements, D. J. (1998), Molecular basis of protein functionality with special
462 consideration of cold-set gels derived from heat-denatured whey, *Trends in Food Science &*
463 *Technology*, **9**, 143-151.

464 Bui, V. T. N. T., Nguyen, B. T., Nicolai, T. & Renou, F. (2019), Mobility of carrageenan chains in iota-
465 and kappa carrageenan gels, *Colloids and Surfaces A: Physicochemical and Engineering Aspects*, **562**,
466 113-118.

467 Croguennoc, P., Meunier, V., Durand, D. & Nicolai, T. (2000), Characterization of semidilute κ -
468 carrageenan solutions, *Macromolecules*, **33**, 7471-7474.

469 De Jong, S., Klok, H. J. & Van de Velde, F. (2009), The mechanism behind microstructure formation in
470 mixed whey protein-polysaccharide cold-set gels, *Food Hydrocolloids*, **23**, 755-764.

471 de Jong, S. & van de Velde, F. (2007), Charge density of polysaccharide controls microstructure and
472 large deformation properties of mixed gels, *Food Hydrocolloids*, **21**, 1172-1187.

473 Heilig, A., Göggerle, A. & Hinrichs, J. (2009), Multiphase visualisation of fat containing β -lactoglobulin-
474 κ -carrageenan gels by confocal scanning laser microscopy, using a novel dye, V03-01136, for fat
475 staining, *LWT - Food Science and Technology*, **42**, 646-653.

476 Inthavong, W., Nicolai, T. & Chassenieux, C. (2018), Polymer Probe Diffusion in Globular Protein Gels
477 and Aggregate Suspensions, *The Journal of Physical Chemistry B*, **122**, 8075-8081.

478 Kharlamova, A., Chassenieux, C. & Nicolai, T. (2018), Acid-induced gelation of whey protein
479 aggregates: Kinetics, gel structure and rheological properties, *Food Hydrocolloids*, **81**, 263-272.

480 Kharlamova, A., Nicolai, T. & Chassenieux, C. (2018), Calcium-induced gelation of whey protein
481 aggregates: Kinetics, structure and rheological properties, *Food Hydrocolloids*, **79**, 145-157.

482 Liu, D., Zhou, P., Nicolai, T. (2020), Effect of Kappa Carrageenan on Acid-induced Gelation of Whey
483 Protein Aggregates. Part I: Potentiometric Titration, Rheology and Turbidity, *Food Hydrocolloids*

484 Nguyen, B. T., Nicolai, T., Chassenieux, C. & Benyahia, L. (2014), The effect of protein aggregate
485 morphology on phase separation in mixtures with polysaccharides, *Journal of Physics: Condensed*
486 *Matter*, **26**, 464102.

487

488 Nicolai, T. (2019), Gelation of food protein-protein mixtures, *Advances in Colloid and Interface*
489 *Science*,**270**, 147-164
490 Soumpasis, D. M. (1983), Theoretical analysis of fluorescence photobleaching recovery experiments,
491 *Biophysical journal*, **41**, 95-97.
492
493
494

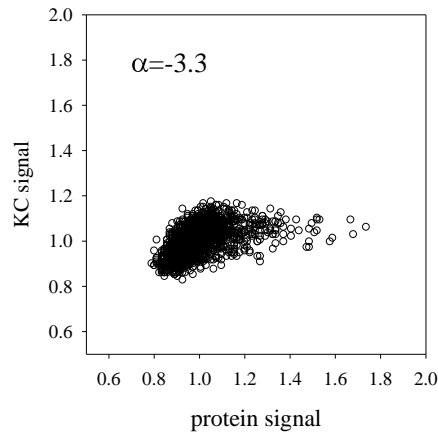
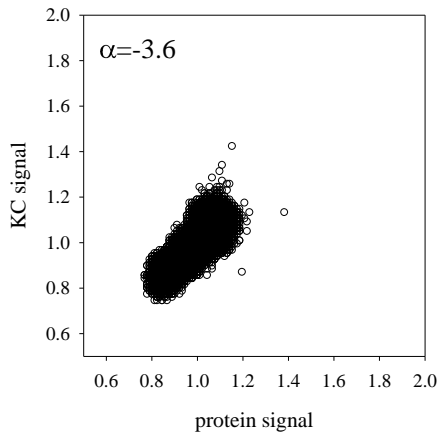
495

Supplementary Information

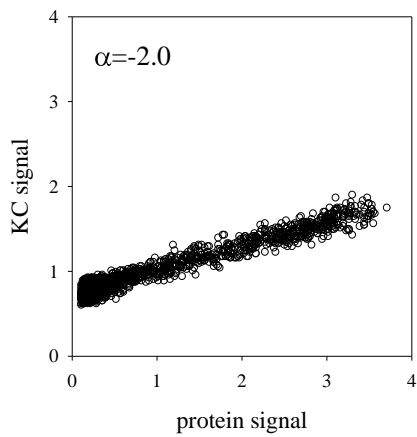
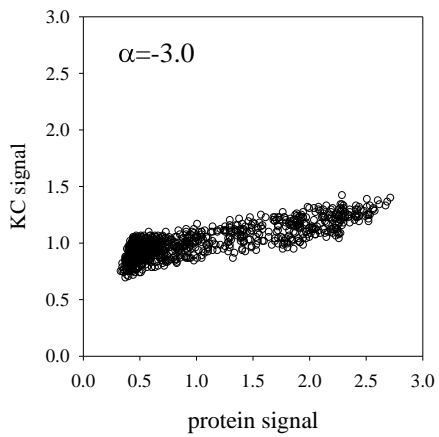
496 Effect of Kappa Carrageenan on Acid-induced Gelation of Whey Protein Aggregates. Part II:

497 Microstructure ,

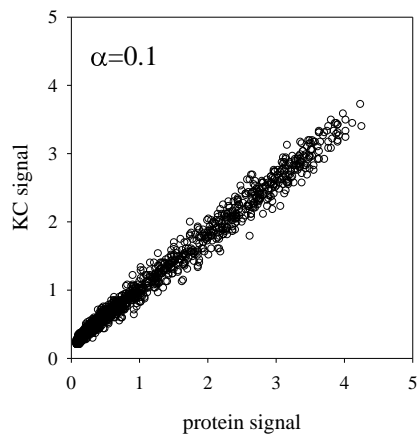
498 Dasong Liu, Peng Zhou, Taco Nicolai



499



500

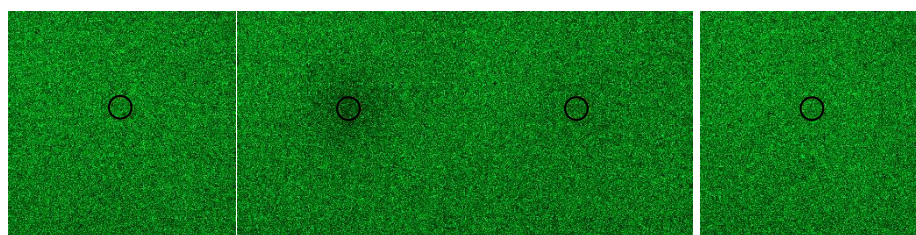


501

502 Fig. S1. Co-localization plots of the KC signal vs the protein signal normalized by the average

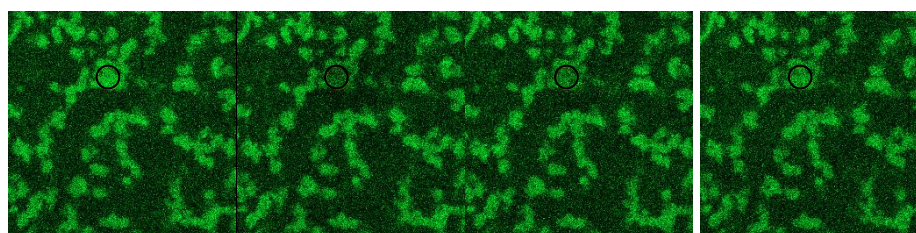
503 intensity for mixtures of 20 g/L WPA and 2 g/L KC at different α . Notice the change in scale.

504



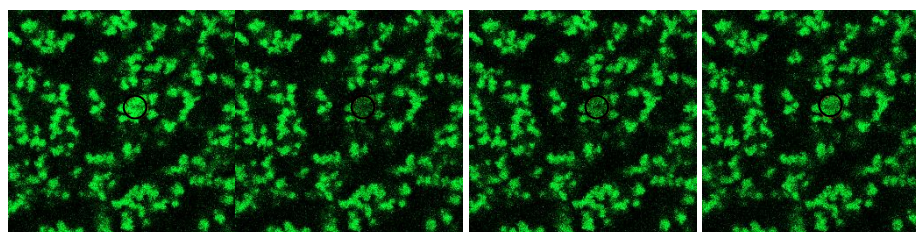
$\alpha = -3.6$

505



$\alpha = -2$

506



$\alpha = 4.8$

507

508

509 Fig. S2. CLSM images taken during FRAP measurements for mixtures of 20 g/L WPA and 2
510 g/L KC at different values of α indicated in the figure. The bleached area with diameter 10
511 μm is indicated by a black circle. The images from left to right were taken before bleaching,
512 and 0.3 s, 33 s and 90 min after bleaching